Theoretical and Mathematical Physics, **203**(1): 535–546 (2020)

NONLINEAR AMPLIFICATION OF OCEAN WAVES IN STRAITS

A. N. Pushkarev[*†] **and V. E. Zakharov**[*‡]

Using the exact Hasselmann equation, we study wind-driven deep-water ocean waves in a strait with the wind directed orthogonally to the shore. The strait has "dissipative" shores with no reflection from the shorelines. We show that the evolution of wave turbulence can be divided into two different regimes in time. During the first regime, waves propagate with the wind, and the wind-driven sea can be described by self-similar solutions of the Hasselmann equation. The second regime starts after a sufficiently significant accumulation of wave energy at the downwind boundary. From this instant, an ensemble of waves propagating against the wind starts to form. Moreover, waves orthogonal to the wind arise and propagate along the strait. The wave system eventually reaches an asymptotic stationary state in which two types of wave motion coexist: an ensemble of self-similar waves propagating with the wind and quasimonochromatic waves propagating almost orthogonally to the wind direction and tending to slant against the wind at the angle of 15° *with respect to the shore of turbulence origination. These "secondary waves" arise only as a result of an intensive nonlinear wave interaction. The total wave energy exceeds its expected value approximately by a factor of two compared with the energy calculated in the absence of shores. We expect that this amplification increases substantially in the presence of reflective shores. We propose calling this "secondary" laser-like mechanism "nonlinear ocean wave amplification"* (*abbreviated NOWA*).

Keywords: nonlinear wave, weak turbulence, ocean surface wave, kinetic wave equation

DOI: 10.1134/S0040577920040091

1. Introduction

It is known that geophysical phenomena strongly influence the course of human history. One relatively recent example is the 1944 allied invasion of Normandy during World War II in Operation Overlord, the largest seaborne invasion in history. The necessary conditions for the landing required definite weather, sea waves, lunar phase, and tides, and only a few days in the month seemed suitable. During the invasion, partially because of poor forecasting, rough seas significantly contributed to allied casualties reaching at least 10,000 including 4,414 dead.

In our current research, we try to elucidate the specificity of wind sea development in ocean straits. While the opinion is widespread in the oceanographic community that we have all necessary research tools including operational wave-forecasting models and parallel computers, we show that there are still new

[*]Skoltech, Moscow, Russia.

[†]Lebedev Physical Institute, RAS, Moscow, Russia, e-mail: dr.push@gmail.com.

[‡]University of Arizona, Tucson, Arizona, USA.

This research was supported by a grant from the Russian Science Foundation (Project No. 19-72-30028).

Prepared from an English manuscript submitted by the authors; for the Russian version, see *Teoreticheskaya i Matematicheskaya Fizika*, Vol. 203, No. 1, pp. 119–133, April, 2020. Received August 30, 2019. Revised August 30, 2019. Accepted October 2, 2019.

0040-5779/20/2031-0535 © 2020 Pleiades Publishing, Ltd.

aspects of the related underlying physics whose understanding is highly desirable for properly constructing wave-forecasting models.

Modern ocean wave forecasting begins with the statistical theory of wind-driven water-surface gravity waves described by the kinetic equation (HE) [1]

$$\frac{\partial \varepsilon}{\partial t}+\frac{\partial \omega_k}{\partial \vec{k}}\frac{\partial \varepsilon}{\partial \vec{r}}=S_{\mathrm{nl}}+S_{\mathrm{in}}+S_{\mathrm{diss}}, \tag{1}$$

where $\varepsilon=\varepsilon(\omega_k,\theta,\vec{r},t)$ is the wave energy spectrum as a function of the wave dispersion $\omega_k=\omega(k)$, angle θ, two-dimensional real space coordinate $\vec{r}=(x,y)$, and time t. In (1), S_{nl}, S_{in}, and S_{diss} are the respective nonlinear, wind input, and wave-breaking dissipation source terms. Hereafter, we consider only the deep-water case $\omega=\sqrt{gk}$, where g is the acceleration of gravity and $k=|\vec{k}|$ is the absolute value of the vector wavenumber $\vec{k}=(k_x,k_y)$.

It is widely accepted that Eq. (1) is already a well-studied object, especially in the considered deep-water case, and that further efforts must be concentrated on improving the simulation with extremely high hurricane winds, the influence of bottom friction, and corrections related to shallow-water effects.

Here, we show that Eq. (1) even in its “simple” form nevertheless deserves further detailed study, which can reveal previously unknown physical effects. Such implications are related to the presence of boundary conditions in real space, such as shore lines in straits, and also to the need to use an exact nonlinear interaction source term S_{nl} instead of the commonly used, computationally more effective DIA surrogate. As we show below, these considerations can significantly modify the seemingly already well-understood picture of the physics of wind-driven surface-wave turbulence in bounded and unbounded domains.

1.1. Recent progress in developing physically justified HE source terms in unbounded domains. Numerical comparisons of different historically developed source terms S_{in} shows a scatter up to a factor of five (see [2], [3]). The situation is no better with the wave energy dissipation source term S_{diss}. As a result, modern operational wave-forecasting models are governed by more than two dozen tuning parameters. A pertinent detailed analysis can be found in [3].

The step toward creating tuning-free wave-forecasting models was taken in [4], [5]. Equation (1) in the stationary limited-fetch approximation

$$\frac{1}{2}\frac{g\cos\theta}{\omega}\frac{\partial \varepsilon}{\partial x}=S_{\mathrm{nl}}+S_{\mathrm{wind}} \tag{2}$$

has been analyzed for self-similar solutions $\varepsilon=x^{p+q}F(\omega x^q,\theta)$. Here, x is the coordinate of the axis $\vec{k}=(k,\theta)$ orthogonal to the shoreline (in physical oceanography, x is called the “fetch”). Under the assumption of a power-law dependence $S_{\mathrm{in}}\sim\omega^{s+1}f(\theta)$ of the wind pumping term on the frequency, those studies yielded the parameter values

$$q=\frac{1}{2+s},\qquad p=\frac{8-s}{2(2+s)} \tag{3}$$

and the “magic relation” $10q-2p=1$. Relations (3) are incomplete and need additional conditions. For this, we introduce the experimental regression line [6], which we use to obtain specific values of the indices defining the Zakharov–Resio–Pushkarev (ZRP) model [4], [5]:

$$s=\frac{4}{3},\qquad p=1,\qquad q=\frac{3}{10},\qquad S_{\mathrm{in}}\sim\omega^{7/3}. \tag{4}$$

Equation (2) gives the dependences of the total energy and the mean frequency on the fetch coordinate:

$$E(x)=E_0x^p, \tag{5}$$

$$\langle\omega(x)\rangle=\omega_0x^{-q}. \tag{6}$$

The ZRP model reproduces a dozen field experiments on limited-fetch waves analyzed in [7] and also self-similar dependences (4)–(6) and does not require tuning with changes of wind speed from 5 m/s to 10 m/s [5]. While the ZRP approach is not completely tuning-free, because it contains two tuning parameters in the wind input term S_{in}, it can be regarded as a step toward a physically justified model of HE (1).

The mentioned facts argue in favor of the ZRP model as a basis for the numerical HE simulation presented here.

2. HE simulation in bounded domains

The self-similar theory described above should be used with care to describe surface-wave turbulence in bounded domains such as ocean straits. It is intuitively understandable that a sign change in the energy advection velocity combined with a four-wave nonlinear interaction under conditions of wave energy concentration at specific locations can modify the self-similar picture of wave turbulence in unbounded domains. Because the considered problem is complicated, numerical simulation tools play a basic role in trying to understand the correct physical mechanisms in such situations.

It was shown in [8]–[10] that a wind blowing perpendicular to the shorelines in an infinitely extended strait excites quasimonochromatic standing waves orthogonal to the wind direction in addition to the traditional wind sea. When the asymptotic turbulent stationary state is attained, the amplitude of the excited quasimonochromatic waves exceeds the maximum spectral peak of the wind sea up to eight times. Here, we elaborate the details of this previously reported phenomenon and also present a mathematical formulation and attempt to understand the underlying physics.

We first consider the problem geometry and formulate simple but physically justified boundary conditions for the corresponding Cauchy problem. For formulating and understanding the problem setup, we find the concept of "pipelines" in a mixed real and Fourier space productive for interpreting energy advection in different directions with respect to the blowing wind. We next describe the model used for the numerical simulation. Finally, we describe and discuss the integral and spectral characteristics of the studied surface-wave turbulence obtained as a result of numerical simulation and also similarities and differences between the already known self-similar regime and the newly observed regime of wave turbulence.

2.1. Cauchy problem statement. We consider the Cauchy problem for the one-dimensional time-dependent version of Eq. (1)

$$\frac{\partial \varepsilon}{\partial t} + \frac{g}{2\omega}\cos\theta\frac{\partial \varepsilon}{\partial x} = S_{\mathrm{nl}} + S_{\mathrm{in}} + S_{\mathrm{diss}}. \tag{7}$$

It is assumed that $\varepsilon = \varepsilon(\omega_k, \theta, x, t)$, where x is the fetch, the wave vector $\vec{k} = (k, \theta)$ is two-dimensional and is defined by its modulus $k = |\vec{k}|$ and the angle θ between $\vec{k}$ and the axis $\vec{x}$. The problem is homogeneous in the direction orthogonal to $\vec{x}$. For convenience, we call the left shoreline the west coast and the right shoreline the east coast. The corresponding domain of length L in the real space between the west and east coasts is represented schematically in Fig. 1. We assume that the wind speed $\vec{U}$ is constant in the direction of $\vec{x}$.

We present a schematic description of the mixed real and Fourier space of the considered system in Fig. 2. The advection group velocity before the spatial derivative $(g/2\omega)\cos\theta$ in Eq. (7) has different signs for waves propagating with and against the wind. The corresponding domain is shown as a two-color cylinder: the darker part corresponds to the positive advection velocity (from the west to the east coast), and the lighter part corresponds to the negative advection velocity directed with the arrow. This schematic picture suggests that the limited-fetch wave consists of three processes in real and Fourier spaces:

- wave energy advection in the fetch direction (darker part of the tube),

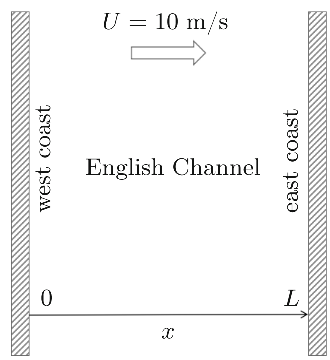

Fig. 1. Schematic representation of the simulation domain in real space: the constant wind speed in the direction of the fetch axis $\vec{x}$ is $U = 10\,\mathrm{m/s}$, and the width of the strait is $L = 40\,\mathrm{km}$.

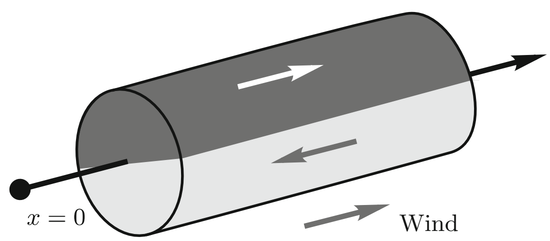

Fig. 2. Schematic description of the propagation of wave energy fluxes along the fetch in the real and Fourier space.

- wave energy advection against the fetch direction (lighter part of the tube), and
- nonlinear interaction of the waves between the darker and lighter parts of the tube in the Fourier space at any given fetch point and time of the space $(\vec{x}, t)$.

Such splitting with respect to physical processes is the basis for our numerical algorithm for solving the HE.

We consider the boundary conditions of the presented problem. We assume that waves with the wave-vector component $\vec{k}$ in the wind direction $\vec{U}$ and therefore propagating in the upper darker half-cylinder have a zero amplitude at the beginning $x = 0$ of the fetch (i.e., at the west coast or on the upper half-circle at the left end of the cylinder in Fig. 2):

$$\varepsilon(\omega, \theta, x, t)|_{x=0} = 0, \quad -\pi/2 < \theta < \pi/2. \tag{8}$$

We call these boundary conditions dissipative. We assume that waves with the wave-vector component $\vec{k}$ in the direction opposite to the wind $\vec{U}$ and therefore propagating in the lower lighter half-cylinder have a zero amplitude at the end $x = L$ of the fetch (i.e., at the east coast or on the lower half-circle at the right end of the cylinder in Fig. 2):

$$\varepsilon(\omega, \theta, x, t)|_{x=L} = 0, \quad \pi/2 < \theta < 3\pi/2. \tag{9}$$

There is no need to define any boundary conditions on the other half-circles at the cylinder ends because the incoming waves are freely advected through the corresponding boundary.

Such boundary conditions have the physical interpretation of perfect absorption of incoming waves at the coasts without any reflection from them; for example, pebble beaches perfectly absorb wave energy without any wave generation or reflection from them. A similar dissipative type of boundary conditions can be observed in nature and in experimental laboratory wave tanks.

For the initial conditions, we assume that the energy distribution has the form of low-level white noise for waves running in the wind direction,

$$\varepsilon(\omega,\theta,x,t)|_{t=0} = 10^{-6}, \quad -\pi/2 < \theta < \pi/2, \tag{10}$$

and is zero for waves running against the wind in the lower lighter cylinder,

$$\varepsilon(\omega,\theta,x,t)|_{t=0} = 0, \quad \pi/2 < \theta < 3\pi/2. \tag{11}$$

Such initial conditions ensure a negligibly small nonlinear interaction at the beginning of the numerical simulation.

3. Numerical simulation

3.1. Discretization algorithm. Equation (7) was solved numerically by the method of splitting with respect to physical processes [11]: the advection, the nonlinear interaction S_{nl}, the wind input S_{in}, and the dissipation S_{diss} due to wave breaking. The corresponding terms were regarded as different physical processes determining the right-hand side of the discretized equation, while the derivative with respect to time was in the left-hand side. The advection term was approximated by a "rectangle" second-order numerical scheme unconditionally stable in space and time [12], the S_{nl} term was solved by the Webb–Resio–Tracy method [13], [14], the wind input term was integrated analytically, and wave-breaking high-frequency energy dissipation was taken into account in the implicit form as a Phillips continuation $\sim \omega^{-5}$ of the dynamical part of the wave spectrum, adjusted at every time step. The time advance was accomplished by an explicit first-order numerical integration scheme.

The initial conditions were given as a seeding wave with a negligibly small nonlinearity and distribution (10) with respect to frequencies and angles for waves running with the wind (in the upper part of the cylinder in Fig. 2) and as zero for waves running against the wind (in the lower part of the cylinder; see Sec. 2.1).

The exact expression for S_{nl} was used in the calculations. To account for wave-breaking energy absorption, an implicit wave-energy dissipation function S_{diss} [3]–[5] was introduced as a spectral continuation in the form of a Phillips tail $\sim \omega^{-5}$.

3.2. Wind wave energy input and wave-breaking dissipation terms. The wind energy input source function S_{in} was chosen in the ZRP form [3]–[5]

$$S_{\mathrm{in}}(\omega,\theta) = \gamma(\omega,\theta)\varepsilon(\omega,\theta), \qquad \omega = 2\pi f, \tag{12}$$

where

$$\gamma(\omega,\theta) = \begin{cases} 0.05\dfrac{\rho_{\mathrm{a}}}{\rho_{\mathrm{w}}}\omega\left(\dfrac{\omega}{\omega_0}\right)^{4/3} q(\theta), & f_{\min} \le f \le f_{\mathrm{d}}, \\ 0, & \text{otherwise}, \end{cases} \tag{13}$$

$$f_{\mathrm{d}} = 1.1\,\mathrm{Hz}, \qquad f_{\min} = 0.1\,\mathrm{Hz}, \qquad \omega_0 = \frac{g}{U}, \qquad U = 10\,\mathrm{m/s}, \qquad \frac{\rho_{\mathrm{a}}}{\rho_{\mathrm{w}}} = 1.3\cdot 10^{-3},$$

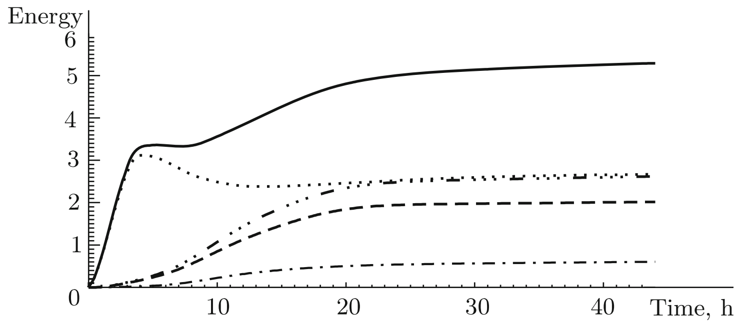

Fig. 3. Total wave energy of the fetch as a function of time – solid line. Wave energy against the wind (light part of the cylinder in Fig. 2) – dashed line; with the wind (dark part of the cylinder in Fig. 2) – dotted line; orthogonal to the wind – dash-dotted line; not in the wind direction – dash-triple-dotted line.

and the function $q(\theta)$ is

$$q(\theta) = \begin{cases} \cos^2\theta, & -\pi/2 \le \theta \le \pi/2, \\ 0, & \text{otherwise}. \end{cases} \tag{14}$$

Here, U is the wind speed at 10 m, and ρ_a and ρ_w are the respective air and water densities. The frequency $f_\mathrm{d} = 1.1$ Hz is taken from [6].

The implicit wave-energy dissipation function S_diss is given as a spectral continuation in the form of a Phillips tail $\sim \omega^{-5}$ starting from the frequency $f_\mathrm{d} = 1.1$ Hz.

3.3. Numerical results. Equation (7) was numerically simulated with the following parameters:

- in the Fourier space in the frequency domain $0.1\,\mathrm{Hz} < f < 2.0\,\mathrm{Hz}$ on a logarithmic grid of 72 points in frequency and a grid of 36 equidistant points in the angle coordinate covering the angle range 2π;
- in the real space, a grid with 40 nodes;
- a fetch size of 40 km, which corresponds to the English Channel.

In Fig. 3, we show the total wave energy of the fetch as a function of time. The plots can be split into two parts: a relatively fast linear rise during about 5 h and a subsequent relatively slow relaxation to a constant asymptotic value. It is quite surprising that the system passes into equilibrium, which means that the channel of wave energy input from the wind is balanced by two channels of wave energy absorption: due to breaking waves and due to dissipation of incoming waves at the coasts.

According to Fig. 3, the total wave energy has the following distribution asymptotically in time: 54% with the wind, 35% against the wind, and 11% orthogonal to the wind. This means that half the energy in the asymptotic equilibrium propagates not in the wind direction. Because the wind input in accordance with Eq. (14) is localized in the angle range $-\pi/2 < \theta < \pi/2$, the appearance of wave energy outside this sector of angles can only be explained by nonlinear wave interaction. We stress that such a "quasi-isotropization" of the wave energy is due to the exact form of S_nl.

3.4. The dynamics of the spectrum in time, Fourier space, and real space. At the early time $t = 2$ h (see Figs. 4 and 5), the energy spectrum has the form of a single hump growing with the distance from the west coast, and the spectral maximum as a function of the fetch has a threshold shape. At the later time $t = 40$ h, which is close to the time of establishing the quasistationary state of the wave system (see Figs. 6 and 7), the shape of the spectrum is rather complicated: in addition to the central

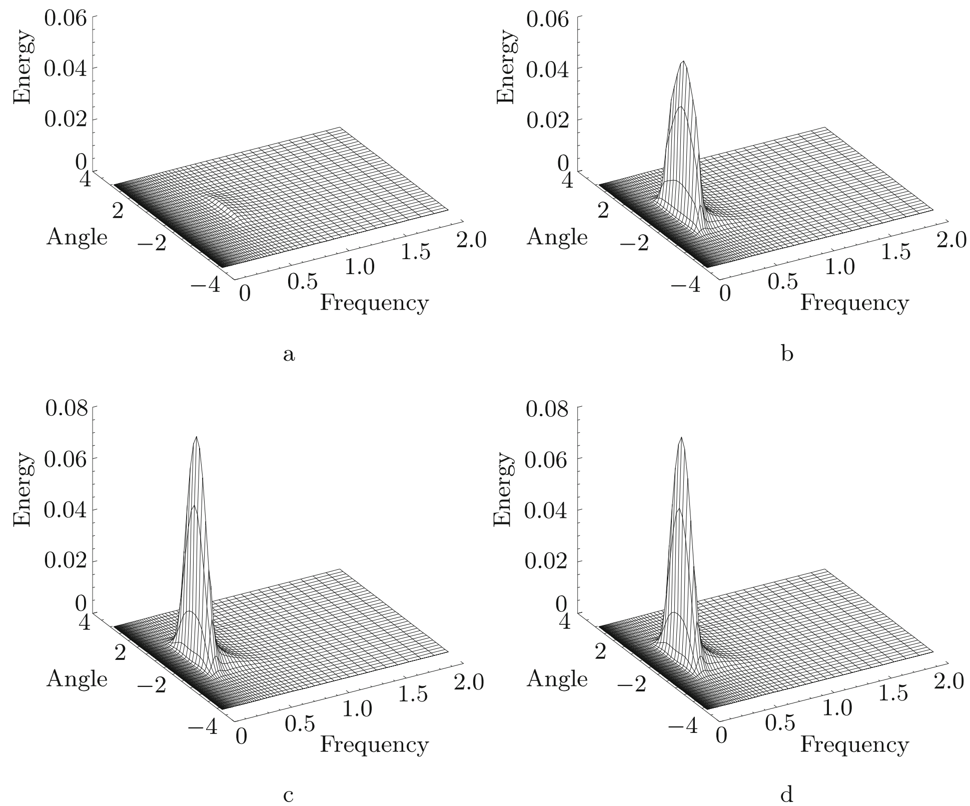

Fig. 4. Spectral distribution of energy as a function of the frequency and angle at the fetch distances (a) 2 km, (b) 14 km, (c) 26 km, and (d) 38 km and the time 2 h.

single-hump energy spectrum of the wind sea growing away from the west coast, we can see powerful side satellites corresponding to waves propagating almost orthogonally to the wind.

This observation is quite remarkable. It means that a sufficiently long excitation of waves by a wind blowing perpendicular to the coasts of a strait asymptotically excites stationary wave turbulence with two components: waves propagating in the wind direction similar to the classical self-similar regime with the single spectral maximum and growing along the fetch from the west to the east coast (we call them the wind sea), and a component consisting of quasimonochromatic waves propagating almost perpendicular to the wind direction. There is a slant of the second wave system with respect to the direction of the coasts; it increases in the direction toward the west coast and reaches the maximum slant of 15° with respect to the coast in the vicinity of the west coast. The formation of this slant could mean that the system adjusts itself such that extra dissipation arises to bring the wave energy system into the balanced stationary state.

All the above consideration unequivocally confirms dividing the system into subsystems in space and in time. It can be seen that the structure of the wave system differs significantly in different time periods: it is unimodal with the single maximum shape for $t < 5$ h and is multimodal for $t > 8$ h, consisting of two quasimonochromatic waves quasiorthogonal to the wind and the single-hump wind sea in the direction of the wind.

We conclude that the wave system in the asymptotic stationary state consists of two subsystems: the first is qualitatively similar to the classical unbounded wave situation without a second boundary, which we call the wind sea, and the second is a standing quasimonochromatic wave directed almost perpendicular to the wind direction.

The described wave system works as a laser-like nonlinear ocean-wave amplifier (abbreviated NOWA) of

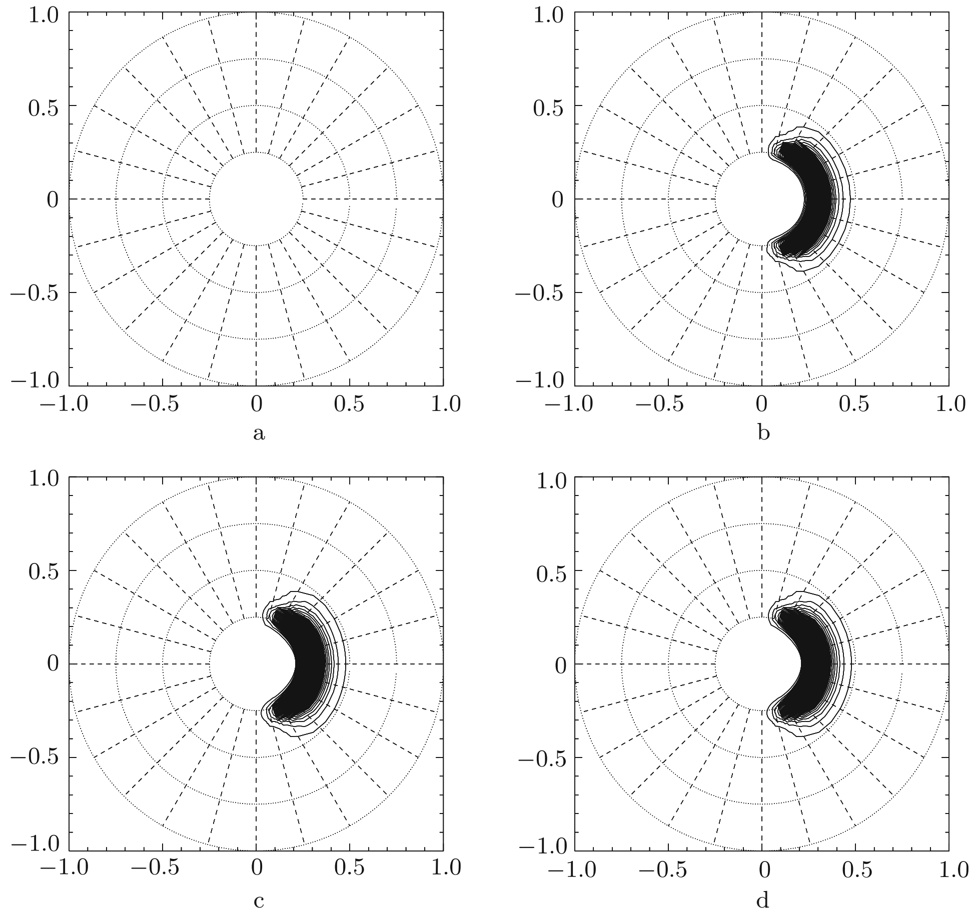

Fig. 5. The same as Fig. 4 in polar coordinates.

quasimonochromatic waves pumped by the orthogonally blowing wind. We note that these quasimonochromatic waves "condense" predominantly near the separatrix of the advection velocity profile, i.e., in the locations where the advection velocity is zero. Such waves have no chance to be advected out of the considered domain to be absorbed at the coasts.

For $t > 8\,\mathrm{h}$, we observe a relatively slow transition of the total wave energy to the asymptotic state, still having the tendency of total wave energy growth from the west coast to east coast although much slower than for the self-similar regime.

In Fig. 8, we show the common logarithm of the wave energy distribution along the fetch at different instants calculated in the angle range $-4\pi/9 < \theta < 4\pi/9$, which takes only the wind sea effects into account and excludes the quasimonochromatic waves. For $t < 5\,\mathrm{h}$, the energy evolution is described by threshold-like function propagating along the fetch and consisting of sloped and horizontal linear parts. For $t \simeq 5\,\mathrm{h}$, the total wave energy distribution along the fetch approaches the self-similar, i.e., linear, form in accordance with Eqs. (4) and (5). Later in time, this dependence slowly evolves to another linear self-similar form with a different slope.

In Fig. 9, we show the common logarithm of the mean frequency distribution along the fetch at different instants calculated in the angle range $-4\pi/9 < \theta < 4\pi/9$. Also in this plot, only the wind sea effects are taken into account, excluding the quasimonochromatic waves. It can be seen that the sloped part of the threshold function propagating from the east to the west coast is close to the self-similar solutions of Eqs. (4)–(6) although the complete correspondence with the self-similar solution along the whole fetch is

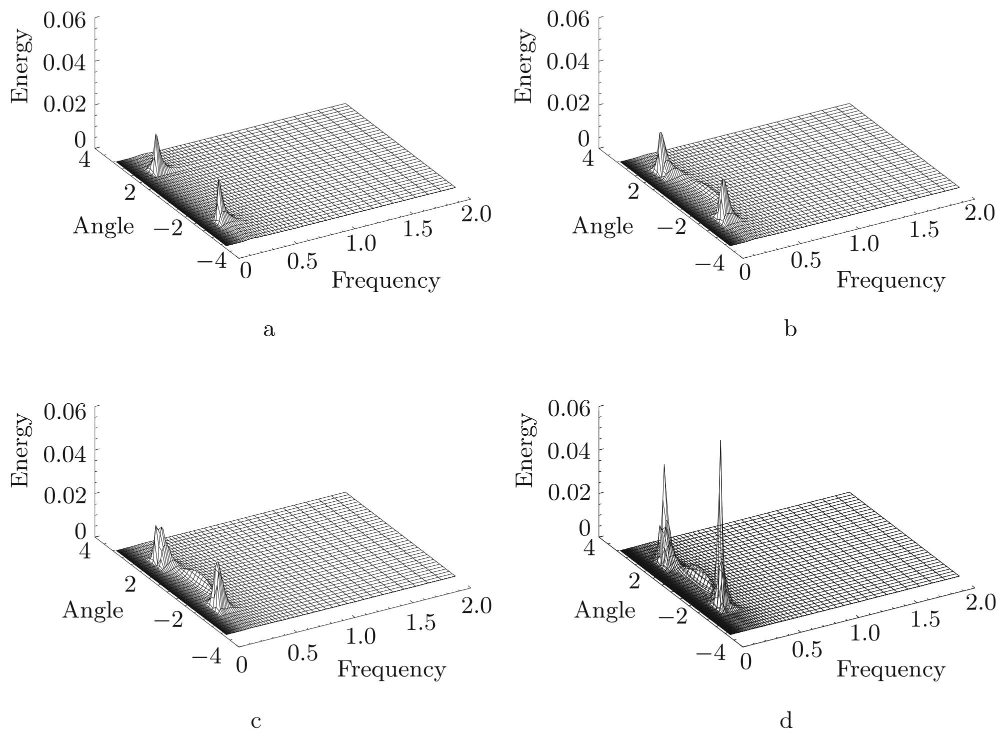

Fig. 6. Spectral distribution of energy as a function of the frequency and angle at the fetch distances (a) 2 km, (b) 14 km, (c) 26 km, and (d) 38 km and the time 40 h.

attained at an earlier time $t = 3\,\mathrm{h}$. This differs from the time $t = 5\,\mathrm{h}$ of reaching the same self-similar solution for the wave energy in Fig. 8. It can be seen that this wind sea distribution is asymptotically closer in time to the classical self-similar form except in the domain of width 3 km close to the west coast. It is quite natural to expect this effect because the intensity of quasimonochromatic waves increases as the west coast is approached together with the degree of their interaction with the wind sea (i.e., interaction of the dark and light parts of the cylinder in Fig. 2), which leads to a deformation of self-similar behavior.

We summarize: the wind sea first relatively quickly realizes an intermediate self-similar asymptotic distribution of energy, which then slowly evolves into the final self-similar state.

4. Conclusions

We have presented results of a numerical simulation of ocean surface-wave turbulence in a strait with a constant wind blowing perpendicular to the coasts. These results show that the problem of limited-fetch growth in straits divides into different processes in space and time.

The initial process consists of propagation of the wave energy front having a threshold shape with sloped and horizontal linear parts. This front in the spectral representation looks like a single hump moving from the west coast to the east coast during characteristic times determined by the ratio of the channel width to the characteristic advection velocity of the spectral peak. This regime is localized in the part of the mixed real and Fourier space corresponding to waves with a positive advection velocity moving with the wind. It is similar to the known self-similar regimes in the case of a limited fetch for unbounded domains.

The second regime occurs later, after the wave energy front reaches the east coast and is initiated by the nonlinear interaction of waves contained in the region of negative advection velocity (lighter part of the cylinder in Fig. 2) with the already formed wave spectrum in the region of positive advection velocity

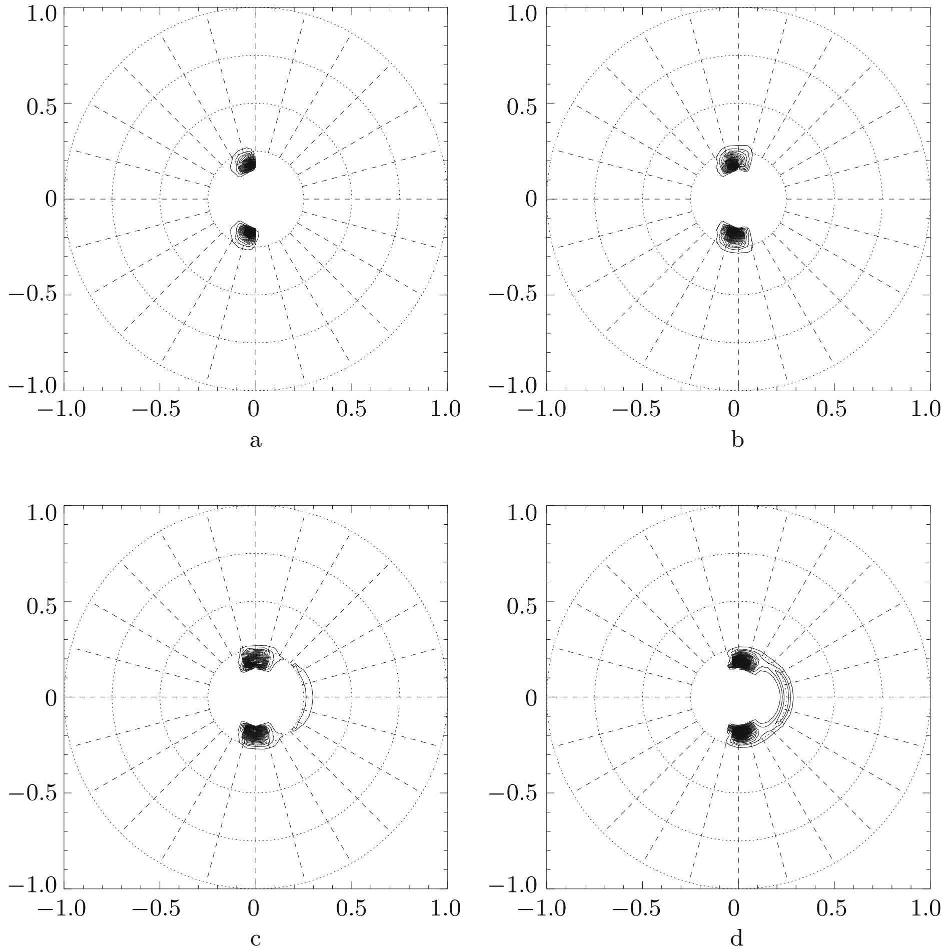

Fig. 7. The same as Fig. 6 in polar coordinates.

(the darker part). The second regime is manifested in the amplification of quasimonochromatic waves propagating orthogonally to the wind. The described wave system works as a NOWA, waves are excited in the direction orthogonal to the wind, and the mechanism of their appearance is apparently predominantly connected with the condensation of wave energy on the separatrix dividing the regions with different signs of the advection velocity.

It is quite surprising that the wave system eventually reaches an asymptotic equilibrium (the "mature sea" state) as the energy coming through the wind input channel is balanced by two other channels of energy dissipation: dissipation by waves breaking and absorption of wave energy at the coasts. The described mechanism for forming a mature sea is a physically well-justified alternative to the dubious concept of a mature sea circulating in the oceanographic literature. The part of the stationary wave energy spectrum closer to the beginning of the fetch tends to slant against the wind at the angle of 15° with respect to the coast. The presence of such waves with a velocity component opposite to the wind is evidence, in particular, that there exists generation of nonlinear waves running against the wind.

We also showed that surface-wave turbulence in straits is separated into the already known self-similar regime of the wind sea and relatively low-frequency quasimonochromatic waves propagating almost orthogonally to the wind.

Asymptotically in time, the part of the wave energy propagating with the wind is approximately equal to the part of the energy propagating perpendicular to and against the wind. This is an important result

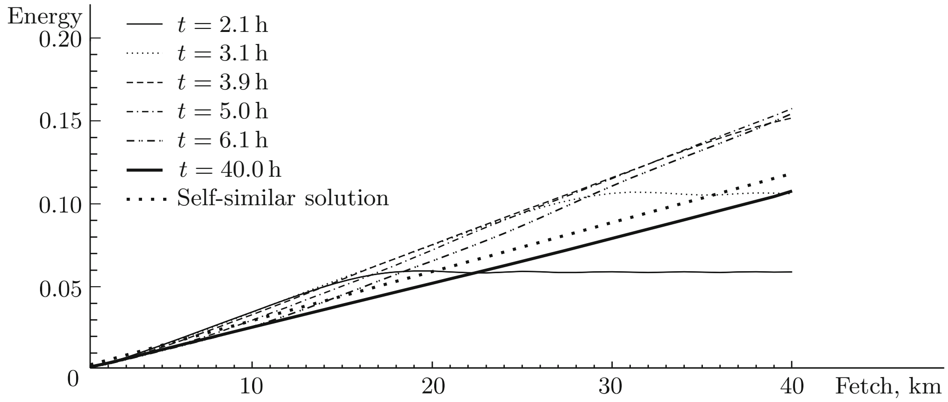

Fig. 8. Common logarithm of the wave energy distribution along the fetch at different instants calculated in the angle range $-80^\circ < \theta < 80^\circ$ with respect to the wind direction $\theta_{\rm wind}$.

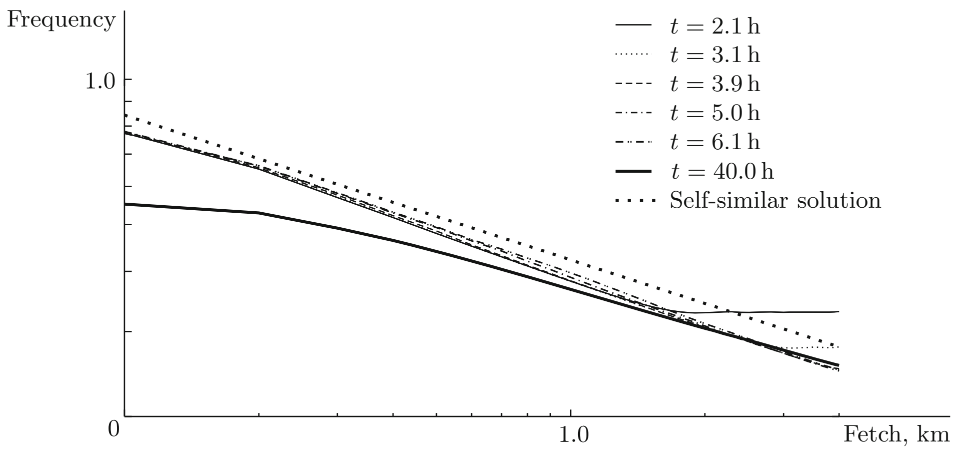

Fig. 9. Common logarithm of the mean frequency distribution as a function of the common logarithm of the fetch at different instants calculated for the angle range $-80^\circ < \theta < 80^\circ$.

of the presented numerical experiments, demonstrating the importance of correctly taking the nonlinear interaction into account, which is responsible for the backscattering of the wind-driven waves and also for the generation of quasimonochromatic waves propagating orthogonally to the wind.

The obtained results have numerous consequences. First of all, they are promising from the standpoint of explaining seiches, which present a significant problem for moored ships in ports, and also predicting the amplitude and localization structure in confined basins. One more lesson from the presented research is that it emphasizes the importance of correctly understanding effects of the boundary conditions inevitably existing in wave-forecasting models; the influence of these conditions should not be interpreted as numerical artifacts. Our further research plan includes taking reflection from the coast into account, and we expect strong amplification of the NOWA effect as a result.

Conflicts of interest. The authors declare no conflicts of interest.

REFERENCES

1. K. Hasselmann, "On the non-linear energy transfer in a gravity-wave spectrum: Part 1. General theory," *J. Fluid Mech.*, **12**, 481–500 (1962); "On the non-linear energy transfer in a gravity wave spectrum: Part 2. Conservation

theorems; wave-particle analogy; irrevesibility," *J. Fluid Mech.*, **15**, 273–281 (1963).

2. S. I. Badulin, A. N. Pushkarev, D. T. Resio, and V. E. Zakharov, "Self-similarity of wind-driven seas," *Nonlin. Processes Geophys.*, **12**, 891–945 (2005).
3. A. Pushkarev and V. Zakharov, "Limited fetch revisited: Comparison of wind input terms, in surface wave modeling," *Ocean Model.*, **103**, 18–37 (2016).
4. V. E. Zakharov, D. Resio, and A. Pushkarev, "New wind input term consistent with experimental, theoretical, and numerical considerations," arXiv:1212.1069v1 [physics.ao-ph] (2012).
5. V. Zakharov, D. Resio, and A. Pushkarev, "Balanced source terms for wave generation within the Hasselmann equation," *Nonlin. Processes Geophys.*, **24**, 581–597 (2017).
6. C. E. Long and D. T. Resio, "Wind wave spectral observations in Currituck Sound, North Carolina," *J. Geophys. Res.*, **112**, C05001 (2007).
7. S. I. Badulin, A. V. Babanin, V. E. Zakharov, and D. T. Resio, "Weakly turbulent laws of wind-wave growth," *J. Fluid Mech.*, **591**, 339–378 (2007).
8. A. Pushkarev, "Nonlinear generation of surface waves against the wind in a limited fetch growth model," *J. Phys.: Conf. Ser.*, **510**, 012048 (2014).
9. V. E. Zakharov and A. N. Pushkarev, "Classical and non-classical regimes of the limited-fetch wave growth and localized structures on the surface of water," Ofc. Naval Res. Grant No. 00014-10-1-0991 report: https://pdfs.semanticscholar.org/d807/9d94d6df29d1e74882a0e2c2593b2d196fbb.pdf (2013).
10. A. N. Pushkarev and V. E. Zakharov, "Nonlinear generation of surface waves against the wind in a limited fetch growth model," in: *Proc. of 20th Meeting WISE* (College Park, Maryland, USA, 21–25 April 2013), ECMWF, Maryland, USA (2013).
11. R. P. Fedorenko, *An Introduction to Computational Physics* [in Russian], MIPT Publ., Moscow (1994).
12. N. N. Kalitkin, *Numerical Methods* [in Russian], Nauka, Moscow (1978).
13. D. J. Webb, "Non-linear transfers between sea waves," *Deep-Sea Res.*, **25**, 279–298 (1978).
14. B.A. Tracy and D. T. Resio, *Theory and Calculation of the Nonlinear Energy Transfer Between Sea Waves in Deep Water*, U. S. Army Engineer Waterways Experiment Station, Vicksburg, Miss. (1982).